Journal of Biomedical Optics

BiomedicalOptics.SPIEDigitalLibrary.org

Effect of probe geometry and optical properties on the sampling depth for diffuse reflectance spectroscopy

Ricky Hennessy
Will Goth
Manu Sharma
Mia K. Markey
James W. Tunnell

SPIE.

Effect of probe geometry and optical properties on the sampling depth for diffuse reflectance spectroscopy

Ricky Hennessy,[a,*] Will Goth,[a] Manu Sharma,[a] Mia K. Markey,[a,b] and James W. Tunnell[a]
[a]University of Texas at Austin, Biomedical Engineering, 107 W. Dean Keeton, Austin, Texas 78712, United States
[b]University of Texas MD Anderson Cancer Center, 1515 Holcombe Boulevard, Houston, Texas 77030, United States

Abstract. The sampling depth of light for diffuse reflectance spectroscopy is analyzed both experimentally and computationally. A Monte Carlo (MC) model was used to investigate the effect of optical properties and probe geometry on sampling depth. MC model estimates of sampling depth show an excellent agreement with experimental measurements over a wide range of optical properties and probe geometries. The MC data are used to define a mathematical expression for sampling depth that is expressed in terms of optical properties and probe geometry parameters. [DOI: 10.1117/1.JBO.19.10.107002]

Keywords: diffuse reflectance spectroscopy; sampling depth; Monte Carlo.

Paper 140486RR received Jul. 28, 2014; revised manuscript received Sep. 18, 2014; accepted for publication Oct. 1, 2014; published online Oct. 27, 2014.

1 Introduction

Diffuse reflectance spectroscopy (DRS) can be used to noninvasively measure tissue optical properties.[1–11] Typically, DRS uses a fiber to inject light into the tissue. The light undergoes scattering and absorption, and the reflected light is collected by a second fiber placed at a short distance, known as the source-detector separation (SDS), from the illumination fiber. The collected light contains quantitative information which can be extracted using an inverse model that relates the collected signal to tissue optical properties.[1,2] Since the reflected light only contains information about the tissue that it passes through, accurate interpretation of the results requires knowledge of the penetration depth. The light penetration depth depends not only on the absorption and scattering properties of the tissue, but also on the geometry of the diffuse reflectance probe.[12] Because of this, the depth sampling of a DRS probe can be tuned by adjusting the probe geometry, allowing for the design of application specific probes.[13]

Many studies have investigated the sampling depth in scattering media both experimentally and numerically.[12–16] Most of these studies rely on the diffusion approximation, which is not valid for short SDSs and highly absorbing media. Others investigated the sampling depth only for reflectance probes with specific geometries, such as single-fiber reflectance,[16] overlapping illumination and collection areas,[17,18] large SDSs (SDS $> 1/\mu_s'$),[19] and diffuse reflectance spectroscopy probes only at specific SDSs and fiber diameters.[13,20] Backman and Gomes recently developed an empirical model to describe sampling depth for a DRS probe. This model is based on a previous study on the sampling depth of single-fiber spectroscopy probes and is only valid for DRS probes with fiber diameters of 200 μm and an SDS of 250 μm.[13] A model that can accurately determine sampling depth for any given SDSs and tissue optical properties will allow the development of application specific probes where light sampling from a specific depth is necessary. Additionally, knowledge of the sampling depth can be used to determine wavelength-dependent differences in the sampling depth due to the difference in optical properties across wavelengths.

In this paper, we analyze the effect of probe geometry and optical properties on the sampling depth using both computational and experimental approaches. First, many Monte Carlo (MC) simulations are performed to determine the sampling depth for a range of optical properties and SDSs. Next, the MC results are validated using a set of phantom experiments. Finally, we develop an analytical expression that can be used to quickly determine the sampling depth for a given SDS, absorption coefficient, and reduced scattering coefficient.

2 Methods

2.1 *Monte Carlo Model*

This study adapts the MC model of light transport in layered tissue code developed by Wang et al.[21] implemented in parallel on a GPU using NVIDIA's compute unified device architecture by Alerstam et al.[22,23] The MC model for modeling light transport is a stochastic method that simulates light transport in a scattering medium with the probabilities of scattering and absorption events determined by the user-specified optical properties of the medium and the geometry of the light source and measurement probe. Photons step sizes were selected from an exponential distribution that depended on the scattering coefficient, and scattering angles were determined by the scattering anisotropy (g) and the phase function. We used the Heyney–Greenstein phase function. Reflection and refraction due to index of refraction mismatch were calculated using the Fresnel equation and Snell's law.

A two-layer model was used with reduced scattering in the bottom layer set to zero, and the absorption in the bottom layer was set to 1×10^{15} cm^{-1} so that photons reaching the bottom layer were terminated. Scattering anisotropy was held constant at 0.85. The sensitivity of photon path length and sampling

*Address all correspondence to: Ricky Hennessy, E-mail: hennessy@utexas.edu

depth to phase function and anisotropy (g) has been explored by Kanick et al. for single-fiber spectroscopy.[16] They performed simulations with $g = [0.8, 0.9, 0.95]$ and with both the Henyey–Greenstein phase function and the modified Henyey–Greenstein phase function. The data showed that path lengths and the sampling depth are independent of anisotropy. The phase function was found to have an observable effect on path length, but the mean sampling depth remained relatively unchanged.

The refractive tissue above the medium was set to 1.452 to match the refractive index of an optical fiber, and the refractive index of the medium was set to 1.33 to match the refractive index of water. The top layer absorption coefficient (μ_a) ranged from 0 to 30 cm^{-1} in 20 increments, the top layer reduced scattering coefficient (μ_s') ranged from 0 to 30 cm^{-1} in 20 increments, and the top layer thickness ranged from 0 to 3000 μm in 250 increments. This gave a total of 100,000 separate MC simulations with each using 10^7 photons. The geometry for the simulations is shown in Fig. 1(a). Spatially resolved reflectance was calculated by convolving the impulse response using a Gaussian-shaped beam profile with radius R_1, and the reflectance signal was calculated by summing the reflectance values centered at the SDS with a collection fiber radius of R_2. For a given set of optical properties (μ_a and μ_s' and probe geometry parameters (SDS, R_1, R_2, we plotted the percentage of photons that never reach depth Z_0 versus Z_0 [Fig. 1(b)]. If we model the curve in Fig. 1(b) as a sigmoid function, the greatest slope will occur at the depth that is reached by 50% of the photons, meaning that the measured reflectance is most sensitive to optical properties at that depth. Because of this, the sampling depth (Z_s) of a probe for a given set of optical properties is defined as the depth reached by 50% of the photons.

2.2 *Empirical Measurements of Sampling Depth*

To validate the computational results, 12 different phantoms were constructed in order to perform an experimental analysis of sampling depth for DRS of varying SDS. The phantoms were composed of 5-mL solutions of water, India ink (Salis International, Golden, Colorado), and scattering microbeads (Polyscienes, Warrington, Pennsylvania), which spanned absorption and scattering values across a range consistent with those normally found in human tissue. Mie theory was used to determine the scattering properties of the 0.99-μm diameter beads. Mix ratios of water and microbeads were determined so that three different scattering spectra from 11 to 25 cm^{-1} were achieved at the reference wavelength of 630 nm. Each of these mix ratios was prepared with four different concentrations of India ink, so that the absorption coefficient for the samples ranged from 0 to 23 cm^{-1}, resulting in 12 total phantoms with different scattering and absorption properties, as seen in Table 1.

Each of these 12 phantoms was placed into a blackened beaker. Reflection measurements were taken while varying the distance between the probe and the bottom of the beaker from 0 to 3 mm in 50-μm increments. Reflectance spectra were collected at wavelengths from 500 to 700 nm and at SDSs of 370, 740, and 1110 μm. Using the known wavelength dependence of scattering and absorption, μ_a and μ_s' were calculated at each wavelength, and for each set of μ_a and μ_s' a plot of P versus Z_0 was created. These plots were then used to calculate Z_s for each set of optical properties.

2.3 *Mathematical Model of Sampling Depth*

The sampling depth for a DRS probe is dependent on the optical properties (μ_a and μ_s' and probe geometry parameters (SDS, R_1, and R_2). The sampling depth data from the MC simulations were accurately described by the equation

$$Z_S = a_1 + a_2\left(\frac{1}{(1+a_3\mu_a)^{a_4}}\right)\left(\frac{1}{(1+a_3\mu_s')^{a_4}}\right). \quad (1)$$

Equation (1) is an empirical expression that accurately describes the MC sampling depth data. This expression was found by trying thousands of candidate functions with the help of TableCurve 2-D (Automated Curve Fitting and Equation Discovery Software, Systat, 2002).

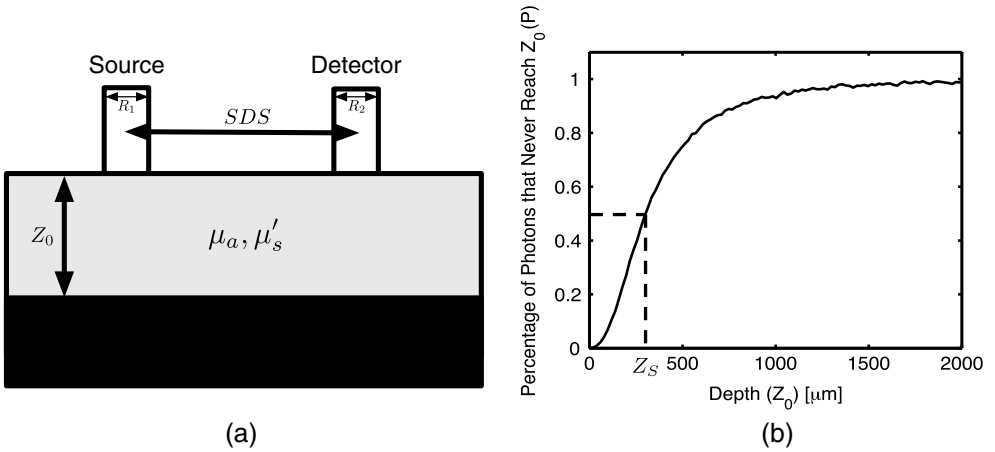

Fig. 1 (a) A two-layer geometry was used for the Monte Carlo (MC) simulations. The bottom layer had an absorption coefficient of 1×10^{15} cm^{-1} and a scattering coefficient of zero so that photons reaching the bottom layer are terminated. Top layer thickness (Z_0) ranged from 0 to 3000 μm in 250 increments, the top layer absorption coefficient (μ_a) ranged from 0 to 30 cm^{-1} in 20 increments. Reflectance measurements were recorded out to 1 cm from the source. (b) A plot of showing the percentage of photons that never reach a depth of Z_0 versus Z_0 with SDS = 300 μm, R_1 = 100 μm, R_2 = 100 μm, μ_a = 1.6 cm^{-1}, and μ_s' = 16 cm^{-1}. Sampling depth (Z_S) is defined as the depth reached by 50% of the photons.

Table 1 Optical properties of phantoms.

Phantom	Reduced scattering at 630 nm (cm^{-1})	Concentration of Ink (volume percentage) (%)
1	11	0.00
2	11	0.15
3	11	0.27
4	11	0.45
5	17	0.00
6	17	0.15
7	17	0.27
8	17	0.45
9	25	0.00
10	25	0.15
11	25	0.27
12	25	0.45

Equation (1) has four free parameters (a_1, a_2, a_3, a_4) whose values must be determined by fitting the MC data. This was accomplished by minimizing the residual between the MC sampling depth results and the sampling depths calculated using Eq. (1) and a Levenberg–Marquardt algorithm scripted in MATLAB®. The dependence of the free parameters on SDS was then determined so that Eq. (1) could be used to determine sampling depth for a given probe geometry and set of optical properties. SDS and Z_S are in units of cm and μ_a and μ_s' are in units of cm^{-1}.

3 Results

3.1 *Experimental Validation*

The sampling depth results from the phantom experiments were used to validate the computational sampling depth results at SDSs of 370, 740, and 1100 μm with optical properties in the range $\mu_a \in [0-25]$ cm^{-1}, and $\mu_s' \in [0-30]$ cm^{-1}. Figure 2 shows an overlay of the computational (transparent mesh) and the experimental (colored surface) results and provides a visual illustration of the good agreement between experimental and computational results. The root-mean-squared percent error for an SDS of 370 μm was 1.71%, for an SDS of 710 μm it was 1.27%, and for 1100 μm it was 1.24%. This agreement indicates that the MC model accurately returns

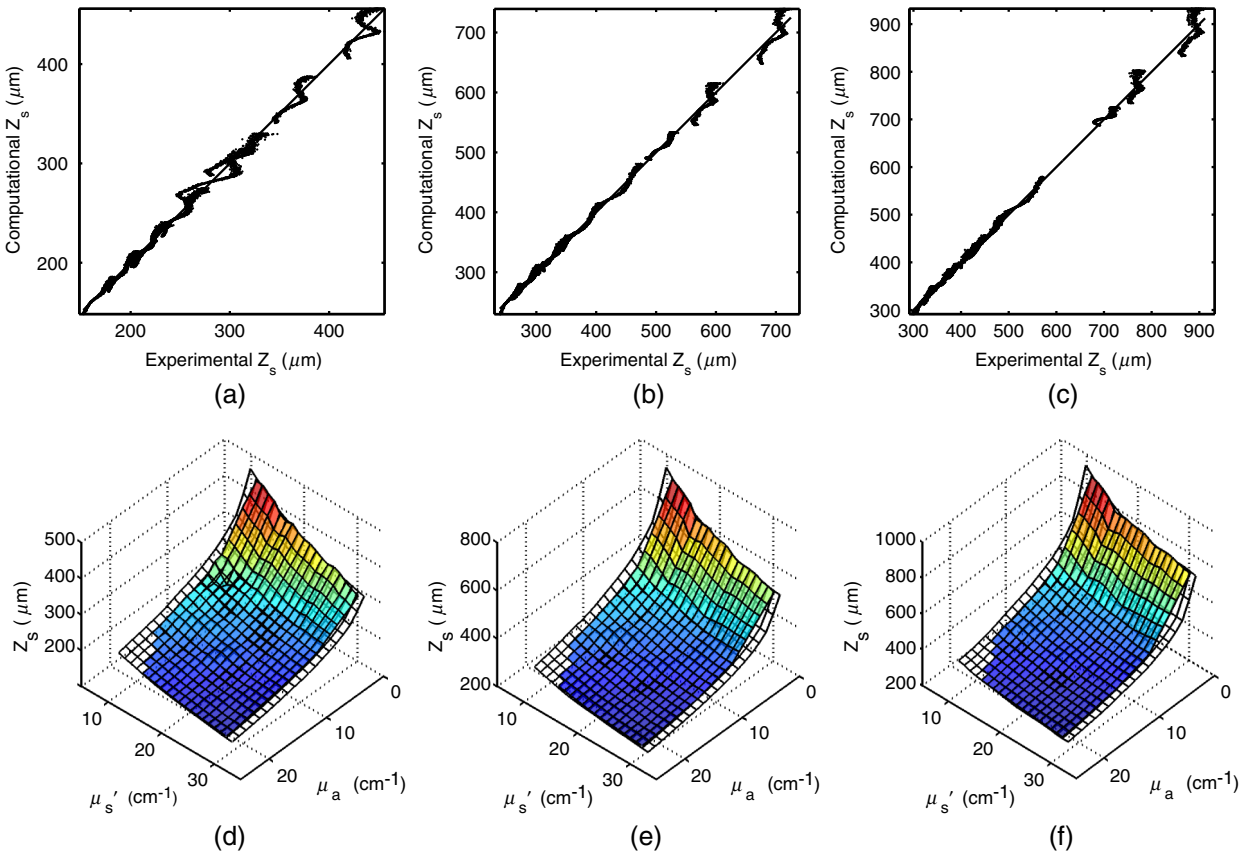

Fig. 2 Plots of Z_S predicted by Monte Carlo modeling versus the experimental values for Z_S at source-detector separations (SDS) of (a) 370, (b) 740, and (c) 1100 μm. An overlay of two-dimensional (2-D) surfaces showing the relationship between scattering and absorption on sampling depth for both Monte Carlo and experimental results. These plots provide a visual illustration of the agreement between the computational (transparent mesh) and experimental (colored surface) results for source-detector separations of (d) 370, (e) 740 and (f) 1100 μm.

Table 2 Values for fitting parameters at various fiber diameters.

Fiber diameter [R_1 and R_2 (μm)]	a_1	a_2	a_3	a_4
50	0.187SDS	1.87SDS + .004	$(2.8\text{SDS} + .16)^2$	0.85
100	0.186SDS	1.83SDS + .01	$(2.55\text{SDS} + .18)^2$	0.85
200	0.183SDS	1.81SDS + .013	$(2.31\text{SDS} + .19)^2$	0.85
400	0.175SDS	1.78SDS + .015	$(1.87\text{SDS} + .22)^2$	0.85

sampling depth. The ripples in the data indicate that the agreement between the phantom measurements and the MC data is wavelength dependent. We believe this is due to the use of the inverse power law for the wavelength dependent description of scattering in the phantoms containing polystyrene microbeads, when in reality, the true scattering values of the phantoms as a function of wavelength contain "humps" in the curve due to the relatively narrow size distribution of the microspheres.

3.2 *Analytical Model of Sampling Depth*

The analytical model of sampling depth shown in Eq. (1) was fit to MC data for a probe with fiber diameters of 50, 100, 200, and 400 μm. For each fiber diameter, SDS ranges from adjacent fibers to 1000 μm, μ_s' ranges from 3 to 40 cm^{-1}, and μ_a ranges from 0 to 40 cm^{-1}. Fitting parameters a_1 and a_2 were found to have a linear relationship with SDS, a_3 was found to have a quadratic relationship with SDS, and a_4 is a constant. Table 2 gives the fitting parameters for the four different common fiber diameters as a function of SDS. Table 2 allows the fitting parameters in Eq. (1) to be determined for a given fiber diameter and SDS so that Eq. (1) can be used to determine sampling depth for a specific probe geometry.

Figure 3 below shows the sampling depth predicted by the analytical model in Eq. (1) and Table 1 versus the MC sampling depth. The ripples in the data indicate that the agreement between the phantom measurements and the MC data is wavelength dependent. We believe this is due to the use of the inverse power law for the wavelength dependent description of scattering in the phantoms containing polystyrene microbeads, when in reality, the true scattering values of the phantoms as a function of wavelength contain "humps" in the curve due to the relatively narrow size distribution of the microspheres.

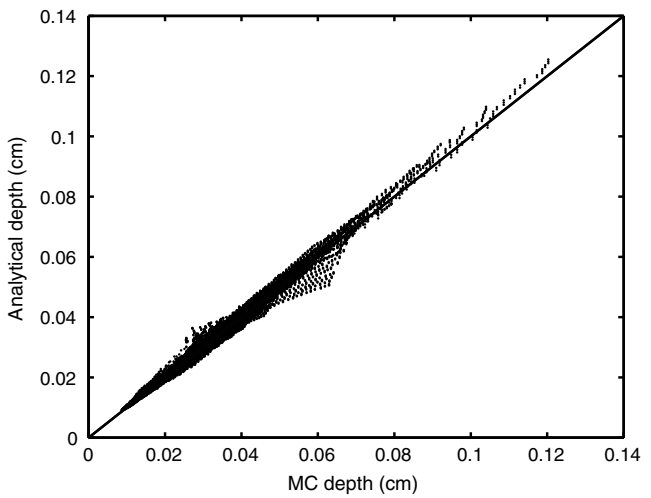

Fig. 3 Monte Carlo results for simulation of sampling depth versus sampling depth predictions from the analytical model for all four fiber diameters [Eq. (1)]. The line of unity is shown for comparative purposes. There is a 2.89% error between the Monte Carlo simulation results and the analytical model results.

3.3 *Effect of Anisotropy and Phase Function on Sampling Depth*

Because scattering anisotropy and the choice of a phase function can impact reflectance at short SDSs,[24] a subset of MC simulations was performed to investigate the effect of anisotropy and phase function on sampling depth. The data showed no change in sampling depth for simulations of different anisotropy values ($g = [0.80, 0.85, 0.90, 0.95]$) over a range of optical properties ($\mu_a \in [0–25]$ cm^{-1}, $\mu_s' \in [0–30]$ cm^{-1}) and probe geometries (SDS $\in [50–800]$ μm), $R \in [50–400]$ μm. This is illustrated in Fig. 4(a), where sampling depth versus SDS is plotted for a probe with 50-μm diameter fibers with a reduced scattering coefficient of 10 cm^{-1} and an absorption coefficient of 10 cm^{-1} for four different anisotropy values. The mean percent error across all anisotropy values for all probe geometries and optical properties was 3.47%. Additionally, the data showed no change in sampling depth for simulations performed with the Heyney–Greenstein (HG) phase function or the modified Heyney–Greenstein (MHG) phase function. This is illustrated in Fig. 4(b), where sampling depth versus SDS is plotted for a probe with 50-μm diameter fibers with anisotropy values of 0.85, a reduced scattering coefficient of 10 cm^{-1} and an absorption coefficient of 10 cm^{-1} for both the HG and MHG phase functions. A change in g or the phase function did affect the reflectance values; however, there was no change in the sampling depth as it is defined in this study. These results agree with the findings by Kanick et al. for single-fiber reflectance spectroscopy[16] that show sampling depth is unaffected by both the anisotropy value and the choice of phase function.

4 Discussion and Conclusions

This study utilizes an MC model to investigate how the optical properties of a turbid media and the geometry of a DRS probe affect sampling depth. This MC model for sampling depth was experimentally validated and was shown to accurately predict sampling depth. We developed an analytical model where sampling depth is expressed in terms of optical properties and probe geometry.

The utility of the model prediction of sampling depth is shown in Fig. 5, which plots sampling depth versus fiber diameter for a probe geometry where the source and detector fibers are adjacent for multiple combinations of optical properties. Figure 5 was created using MC simulation and not the empirical model in Eq. (1). This type of probe geometry accurately models the commonly used 6-around-1 fiber orientation, where a center

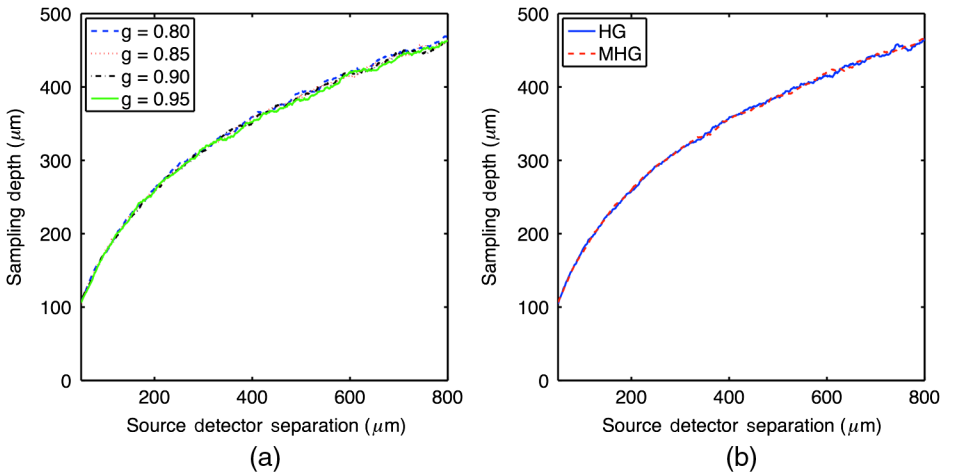

Fig. 4 (a) Sampling depth versus SDS for varying anisotropy values with $\mu_a = 10$ cm^{-1}, $\mu_s' = 10$ cm^{-1}, and fiber diameter at 50 μm. (b) Sampling depth versus SDS for both HG and MHG phase functions with $\mu_a = 10$ cm^{-1}, $\mu_s' = 10$ cm^{-1}, $g = 0.85$ and the fiber diameter at 50 μm.

fiber is used for illumination and six collection fibers of the same size are placed around the illumination fiber. All three series have the same value for scattering ($\mu_s' = 10$ cm^{-1}), and series 1 represents a moderately absorbing tissue ($\mu_a = 10$ cm^{-1}), series 2 represents a highly absorbing tissue ($\mu_a = 20$ cm^{-1}), and series 3 represents a nonabsorbing tissue ($\mu_a = 0$ cm^{-1}). As expected, the sampling depth decreases for increasing absorption. Importantly, a relatively small increase in sampling depth results from a large change in SDS. This is especially evident in the highly absorbing tissue. For example, in series 3 ($\mu_s' = 10$ cm^{-1}), $\mu_a = 20$ cm^{-1}, doubling the fiber diameter from 500 to 1000 μm only increases the sampling depth by 17% (from 240 to 270 μm). This result indicates that the 6-around-1 orientation is best for interrogating shallow depths and that it may not be possible to substantially increase sampling depth by increasing the fiber diameter.

The models developed in this study can also be used to provide an estimate of wavelength-dependent difference in optically sampled tissue volumes, which occurs when optical properties change as a function of wavelength. Figure 6 shows sampling depth as a function of wavelength for a sample containing 1 mg/ml of fully oxygenated hemoglobin at three different SDSs. The reduced scattering coefficient is 20 cm^{-1} across all wavelengths. The models can also be used to explain discrepancies between measurements of tissue with different probe geometries. The main utility of the proposed model is that it can be used to aid the design of application specific DRS probes. For

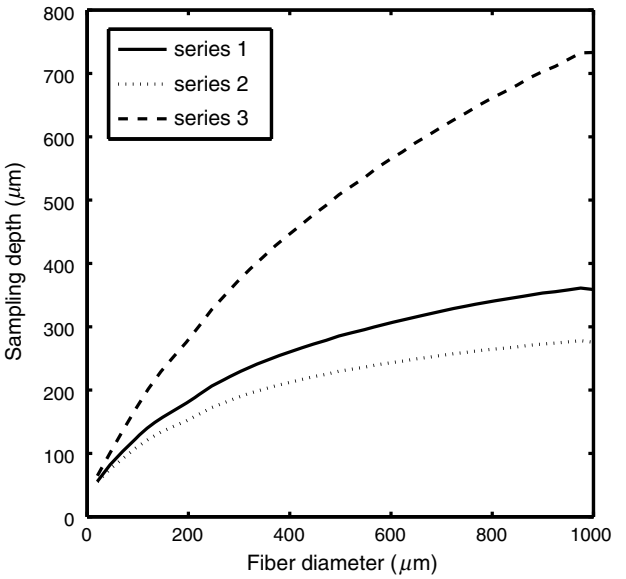

Fig. 5 Mathematical model estimates of sampling depth for adjacent fibers for measurement of mediums containing different optical properties combinations: series 1 ($\mu_a = 10$ cm^{-1}), $\mu_s' = 10$ cm^{-1}, series 2 ($\mu_a = 0$ cm^{-1}), $\mu_s' = 10$ cm^{-1}, series 3 ($\mu_a = 20$ cm^{-1}), $\mu_s' = 10$ cm^{-1}. These data were created using MC simulation and not the empirical model in Eq. (1).

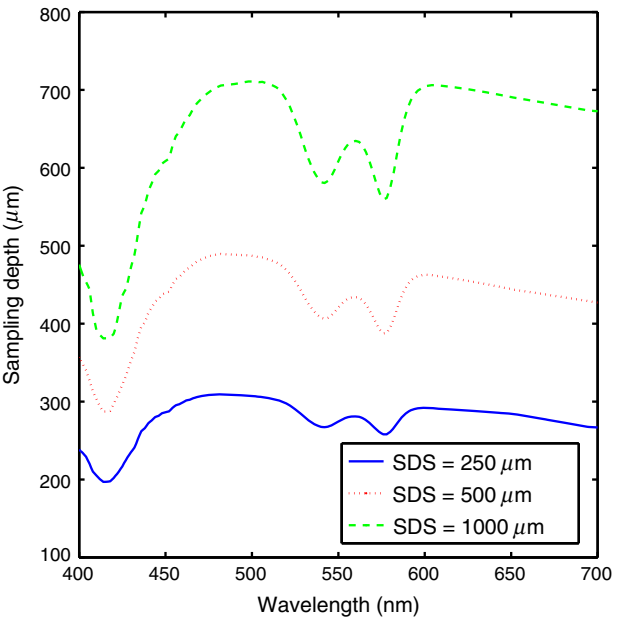

Fig. 6 Sampling depth versus wavelength for a sampling containing 1 mg/ml of fully oxygenated hemoglobin at source detector separations of 250, 500, and 1000 μm. Reduced scattering is 20^{-1} across all wavelengths.

example, to design a probe that measures the properties of the epidermis, one may desire a sampling depth equal to or less than the epidermal thickness (~70 μm[25]) to ensure that most sampled photons only interact with the epidermis and not the dermis. As shown in Fig. 5, achieving a sampling depth of less than 70 μm would require a 6-around-1 fiber orientation with fiber diameters of 50 μm or less.

This study uses an MC model of DRS to investigate the effect of optical properties and probe geometry on the sampling depth of photons collected by a DRS probe. The MC model of sampling depth was experimentally validated and shown to accurately predict sampling depth. An analytical model of sampling depth was developed and is valid for a DRS probe with fiber diameters of 200 μm and for a wide range of SDSs (200 to 1000 μm), absorption coefficients (0 to 40 cm^{-1}), and reduced scattering coefficients (0 to 40 cm^{-1}). The model of sampling depth indicates that for adjacent fibers in the 6-around-1 orientation, the sampling depth cannot be significantly increased by increasing the fiber diameters. This result suggests that deeper sampling depth can only be accomplished by increasing the gap between the source and collection fibers. Future work will involve the application of the sampling depth model to aid in the design of application specific probes that will be used to interrogate the optical properties of specific layers to tissue such as the epidermis and dermis.

References

1. R. Hennessy et al., "Monte Carlo lookup table-based inverse model for extracting optical properties from tissue-simulating phantoms using diffuse reflectance spectroscopy," *J. Biomed. Opt.* **18**(3), 037003 (2013).
2. M. Sharma et al., "Verification of a two-layer inverse Monte Carlo absorption model using multiple source-detector separation diffuse reflectance spectroscopy," *Biomed. Opt. Express* **5**(1), 40–53 (2014).
3. Z. Ge, K. T. Schomacker, and N. S. Nishioka, "Identification of colonic dysplasia and neoplasia by diffuse reflectance spectroscopy and pattern recognition techniques," *Appl. Spectrosc.* **52**(6), 833–839 (1998).
4. F. Koenig et al., "Spectroscopic measurement of diffuse reflectance for enhanced detection of bladder carcinoma," *Urology* **51**(2), 342–345 (1998).
5. G. Zonios et al., "Diffuse reflectance spectroscopy of human adenomatous colon polyps *in vivo*," *Appl. Opt.* **38**(31), 6628–6637 (1999).
6. G. Zonios, J. Bykowski, and N. Kollias, "Skin melanin, hemoglobin, and light scattering properties can be quantitatively assessed *in vivo* using diffuse reflectance spectroscopy," *J. Invest. Dermatol.* **117**(6), 1452–1457 (2001).
7. U. Utzinger and R. Richards-Kortum, "Fiber optic probes for biomedical optical spectroscopy," *J. Biomed. Opt.* **8**(1), 121–147 (2003).
8. N. M. Marin et al., "Diffuse reflectance patterns in cervical spectroscopy," *Gynecol. Oncol.* **99**(3), S116–S120 (2005).
9. B. W. Murphy et al., "Toward the discrimination of early melanoma from common and dysplastic nevus using fiber optic diffuse reflectance spectroscopy," *J. Biomed. Opt.* **10**(6), 064020 (2005).
10. N. Rajaram et al., "Pilot clinical study for quantitative spectral diagnosis of non-melanoma skin cancer," *Lasers Surg. Med.* **42**(10), 716–727 (2010).
11. N. Rajaram, T. H. Nguyen, and J. W. Tunnell, "Lookup table-based inverse model for determining optical properties of turbid media," *J. Biomed. Opt.* **13**(5), 050501 (2008).
12. H. Arimoto, M. Egawa, and Y. Yamada, "Depth profile of diffuse reflectance near-infrared spectroscopy for measurement of water content in skin," *Skin Res. Technol.* **11**(1), 27–35 (2005).
13. A. J. Gomes and V. Backman, "Algorithm for automated selection of application-specific fiber-optic reflectance probes," *J. Biomed. Opt.* **18**(2), 027012 (2013).
14. Y. Tsuchiya, "Photon path distribution and optical responses of turbid media: theoretical analysis based on the microscopic Beer–Lambert law," *Phys. Med. Biol.* **46**(8), 2067–2084 (2001).
15. X. Guo, M. F. G. Wood, and A. Vitkin, "A Monte Carlo study of penetration depth and sampling volume of polarized light in turbid media," *Opt. Commun.* **281**(3), 380–387 (2008).
16. S. C. Kanick et al., "Monte Carlo analysis of single fiber reflectance spectroscopy: photon path length and sampling depth," *Phys. Med. Biol.* **54**(22), 6991–7008 (2009).
17. A. J. Gomes et al., "Monte Carlo model of the penetration depth for polarization gating spectroscopy: influence of illumination-collection geometry and sample optical properties," *Appl. Opt.* **51**(20), 4627–4637 (2012).
18. A. J. Gomes and V. Backman, "Analytical light reflectance models for overlapping illumination and collection area geometries," *Appl. Opt.* **51**(33), 8013–8021 (2012).
19. C. Bonnéry et al., "Changes in diffusion path length with old age in diffuse optical tomography," *J. Biomed. Opt.* **17**(5), 056002 (2012).
20. S. C. Kanick, H. J. Sterenborg, and A. Amelink, "Empirical model description of photon path length for differential path length spectroscopy: combined effect of scattering and absorption," *J. Biomed. Opt.* **13**(6), 064042 (2008).
21. L. Wang, S. L. Jacques, and L. Zheng, "MCML—Monte Carlo modeling of light transport in multi-layered tissues," *Comput. Methods Programs Biomed.* **47**(2), 131–146 (1995).
22. E. Alerstam, T. Svensson, and S. Andersson-Engels, "Parallel computing with graphics processing units for high-speed Monte Carlo simulation of photon migration," *J. Biomed. Opt.* **13**(6), 060504 (2008).
23. E. Alerstam et al., "Next-generation acceleration and code optimization for light transport in turbid media using GPUs," *Biomed. Opt. Express* **1**(2), 658–675 (2010).
24. K. W. Calabro and I. J. Bigio, "Influence of the phase function in generalized diffuse reflectance models: review of current formalisms and novel observations," *J. Biomed. Opt.* **19**(7), 075005 (2014).
25. T. Gambichler et al., "*In vivo* data of epidermal thickness evaluated by optical coherence tomography: effects of age, gender, skin type, and anatomic site," *J. Dermatol. Sci.* **44**(3), 145–52 (2006).

Ricky Hennessy is a NSF graduate research fellow in the Department of Biomedical Engineering at the University of Texas at Austin. He is advised by Drs. James W. Tunnell and Mia K. Markey. He earned a BS and MS in biomedical engineering from California Polytechnic State University in San Luis Obispo. He will be graduating with his PhD in February 2015.

Will Goth is a graduate student in the Department of Biomedical Engineering at the University of Texas at Austin. He is currently advised by Dr. James W. Tunnell in the Bio-Photonics Lab and Dr. Michael S. Sacks in the Center for Cardivascular Simulation, and is a member of SPIE.

Manu Sharma: Biography is not available.

Mia K. Markey is a full professor of biomedical engineering at the University of Texas at Austin and an adjunct associate professor of imaging physics at the University of Texas MD Anderson Cancer Center. A 1994 graduate of the Illinois Mathematics and Science Academy, she received her BS degree in computational biology (1998) from Carnegie Mellon University and her PhD degree in biomedical engineering (2002), along with a certificate in bioinformatics, from Duke University.

James W. Tunnell is an associate professor of biomedical engineering at the University of Texas at Austin. He earned a BS in electrical engineering from the University of Texas and a PhD in bioengineering from Rice University. He was awarded a National Research Service Award from the NIH to fund his postdoctoral fellowship at the MIT from 2003 to 2005. He joined the faculty of the University of Texas in the fall of 2005.